Characterization of the Bis(azido)(*meso*-tetraphenylporphinato)ferrate(III) Anion. An Unusual Spin-Equilibrium System

Mary K. Ellison,[†] Habib Nasri,[†,‡] Y.-M. Xia,[§] Jean-Claude Marchon,[⊥] Charles E. Schulz,*[,||] Peter G. Debrunner,*[,§] and W. Robert Scheidt*[,†]

Department of Chemistry and Biochemistry, University of Notre Dame, Notre Dame, Indiana 46556, Département de Recherche Fondamentale sur la Matière Condensée/SCIB, Laboratoire de Chimie de Coordination (URA CNRS 1194), CEA-Grenoble, 38054 Grenoble, France, and Departments of Physics, Knox College, Galesburg, Illinois 61401, and University of Illinois, Urbana, Illinois 61801

Received May 8, 1997[⊗]

The complex anion bis(azido)(tetraphenylporphinato)ferrate(III) has been synthesized and characterized by variable-temperature X-ray structure determinations, powder and single-crystal EPR, IR, and Mössbauer spectroscopy, and magnetic susceptibility measurements. The synthesis utilizes 18-crown-6 to solubilize sodium azide in the synthetic procedure. All physical data for $[Na(18C6)(H_2O)_2][Fe(TPP)(N_3)_2]\cdot 2C_6H_5Cl$ are consistent with a thermal spin-equilibrium system: low spin ($S = {}^1/_2$) ⇌ high spin ($S = {}^5/_2$). Structure determinations at 130 and 293 K show equatorial and axial Fe−N bond elongation at 293 K. $Fe-N_p = 1.9991(11)$ Å, $Fe-N_{az} = 1.9734(14)$ Å at 130 K, and $Fe-N_p = 2.010(4)$ Å, $Fe-N_{az} = 1.998(2)$ Å at 293 K. The EPR *g* values for a powder sample at 4.2 K are 1.81, 2.18, and 2.70. A fit of the powder EPR spectrum at 4.2 K with a crystal field model that allows quartet and sextet admixtures suggests that the first sextet state is ∼655 cm^{-1} above the ground doublet. Single-crystal EPR data indicate that the largest *g* value occurs at an angle of 56° from the porphyrin normal and at 35 and 81° from the $Fe-N_p$ vectors. The asymmetric azide IR absorption bands at 2014 and 2036 cm^{-1} can be assigned to low- and high-spin species, respectively, and display temperature-dependent intensities. The Mössbauer experiments reveal a gradual decrease in the quadrupole splitting as the temperature increases from 140 to 300 K. The magnetic susceptibility measurements show a gradual increase of μ_{eff} with temperature. Crystal data for $[Na(18C6)(H_2O)_2][Fe(TPP)(N_3)_2]\cdot 2C_6H_5Cl$ (130 K): $a = 11.417(2)$ Å, $b = 12.371(4)$ Å, $c = 12.628(2)$ Å, $\alpha = 64.30(2)°$, $\beta = 77.18(3)°$, $\gamma = 77.67(2)°$, triclinic, space group $P\bar{1}$, $Z = 1$. Crystal data (293 K): $a = 11.7652(12)$ Å, $b = 12.6488(6)$ Å, $c = 12.8608(13)$ Å, $\alpha = 62.02(2)°$, $\beta = 75.996(7)°$, $\gamma = 75.465(9)°$.

Introduction

As part of our studies on the fundamental properties of iron porphyrinates, we have investigated the possible formation of anionic bis(pseudohalide)(porphinato)iron(III) derivatives. There are, to our knowledge, only three previously reported ligand sets that have yielded six-coordinate anionic iron(III) derivatives. Two of these form low-spin derivatives and have the strong-field ligands cyanide[1] or nitrite ion[2] as the two axial ligands. The third is a high-spin species and has the weak-field ligand fluoride as the two axial ligands.[3]

One possible reason for the relatively small number of derivatives are synthetic limitations. The reported syntheses make use of organic-soluble iron porphyrinates and typically water-soluble inorganic salts (the convenient source of anionic ligands), which are effectively incompatible reactants. We report in this paper the use of crown ethers to solubilize an inorganic salt in organic solvents typically used with iron porphyrinates. The use of this procedure with sodium azide and 18-crown-6 provides, for some iron(III) porphyrinate derivatives, a convenient synthesis of bis(azido)iron(III) porphyrinate derivatives. The preliminary characterization of one such derivative, bis(azido)(tetraphenylporphinato)ferrate(III), suggested that it had interesting magnetic properties.

We report in this paper the complete characterization of this anionic complex as its sodium(18-C-6) salt. Characterization includes crystal structure determinations at 293 and 130 K, temperature-dependent IR and Mössbauer spectroscopy, and powder and single-crystal EPR spectroscopy.[4] All characterization results for $[Na(18C6)(H_2O)_2][Fe(TPP)(N_3)_2]\cdot 2C_6H_5Cl$ are consistent with the description of the iron complex as a thermal spin-equilibrium system: low spin ($S = {}^1/_2$) ⇌ high spin ($S = {}^5/_2$). Accordingly, we have fitted the EPR spectra with a three-term crystal-field model based on earlier work of Ristau.[5] Among other things, the model allows the estimation of the doublet-sextet energy gap as ∼655 cm^{-1}. The single-crystal EPR measurements show that the principal axis system of the **g**-tensor is rotated away from the heme normal.

Experimental Section

General Information. 18-Crown-6 (Aldrich) was recrystallized from acetonitrile and dried under vacuum. Tetrahydrofuran was distilled from sodium benzophenone. All other chemicals were used as received from Aldrich or Fisher. Silver triflate was stored and

* Authors for correspondence.
† University of Notre Dame.
‡ Present address: Faculté des Sciences de Monastir, 5000 Monastir, Tunisia.
§ University of Illinois.
⊥ CEA, Grenoble.
|| Knox College.
⊗ Abstract published in *Advance ACS Abstracts,* September 1, 1997.
(1) Scheidt, W. R.; Haller, K. J.; Hatano, K. *J. Am. Chem. Soc.* **1980**, *102*, 3017.
(2) Nasri, H.; Goodwin, J. A.; Scheidt, W. R. *Inorg. Chem.* **1990**, *29*, 185.
(3) Scheidt, W. R.; Lee, Y. L.; Tamai, S.; Hatano, K. *J. Am. Chem. Soc.* **1983**, *105*, 778.

(4) Abbreviations: TPP, $T_{piv}PP$, TMP, and OEP are the dianions of 5,-10,15,20-tetraphenylporphyrin, *meso*-α,α,α,α-tetrakis(*o*-pivalamidophenyl)porphyrin, *meso*-tetramesitylporphyrin, and octaethylporphyrin, respectively; EPR, electron paramagnetic resonance; 18C6, 1,4,7,10,13,16-hexaoxacyclooctadecane (18-crown-6)
(5) Ristau, O. *Acta Biol. Med. Germ.* **1980**, *39*, 71.

S0020-1669(97)00527-2 CCC: $14.00

handled in an inert atmosphere dry box. *meso*-Tetraphenylporphyrin (H_2TPP) was prepared according to Adler et al.[6] [Fe(TPP)Cl] was prepared according to a modified Adler preparation.[7] [Fe(TPP)(OSO_2CF_3)] was prepared from [Fe(TPP)Cl] by anion exchange with $AgOSO_2CF_3$.[8] IR spectra were recorded on a Perkin-Elmer 883 IR spectrophotometer as KBr pellets. EPR powder spectra were recorded on a Bruker 200D X-band spectrometer equipped with an Oxford ESR910 helium flow cryostat. The same instrument was used for single-crystal measurements. Quartz rods with one end ground flat parallel or perpendicular to the axis, respectively, were used for mounting the crystal, and EPR spectra were taken at 4 K as the rod was rotated in 15° steps about its axis perpendicular to the field. The crystal, a plate of roughly 0.6 mm by 0.3 mm on a side was aligned on the quartz flats by eye with an estimated accuracy of a few degrees. Three sets of measurements were taken with nominally orthogonal orientations of the crystal with respect to the axis of rotation. Mössbauer measurements were performed on a constant acceleration spectrometer from 4 to 300 K with optional small field and in a 8.5 T superconducting magnet system (Knox College).

Synthesis of [Na(18C6)(H_2O)$_2$][Fe(TPP)(N_3)$_2$]·2C_6H_5Cl. Sodium azide (320 mg, 4.9 mmol) and 18-crown-6 (1.3 g, 4.9 mmol) were stirred together in chlorobenzene (30 mL). Even with vigorous stirring for several minutes the sodium azide was not completely dissolved. [Fe(TPP)OSO_2CF_3] (200 mg, 0.24 mmol), in chlorobenzene (30 mL), was added to the azide/crown-ether solution and stirred at room temperature for 1 h. X-ray-quality crystals can be obtained either by slow evaporation or by liquid diffusion using hexanes as the nonsolvent. IR ($\nu_{as}(N_3)$, KBr pellet): 2014 and 2036 cm^{-1}.

Sample Preparation for Magnetic Susceptibility and Mössbauer Measurements. Crystals of the bis(azido) complex became coated with excess NaN_3 in the process of crystallization. In order to obtain pure samples for the magnetic susceptibility measurements, the samples were washed with water to remove the salt and dried by flowing argon over the samples. All samples were ground. The Mössbauer samples were immobilized in Apiezon grease and stored at 80 K.

X-ray Structure Determinations. A dark purple, blocklike crystal of [Na(18C6)(H_2O)$_2$][Fe(TPP)(N_3)$_2$]·2C_6H_5Cl (0.53 × 0.67 × 0.73 mm^3), cut from a larger crystal, was used for the structure determination. Data collection was carried out on an Enraf-Nonius FAST area-detector diffractometer with a Mo rotating anode source ($\bar{\lambda}$ = 0.710 73 Å). Our detailed methods and procedures for small molecule X-ray data collection with the FAST system have been described previously.[9] Data collections were performed with the same crystal at 130(2) K and at 293 K. The structure was solved using the direct methods program SHELXS-86;[10] subsequent difference Fourier syntheses led to the location of all the remaining non-hydrogen atoms. The structures were refined against F^2 with the program SHELXL-93,[11] in which all data collected were used including negative intensities. Hydrogen atoms of the porphyrin ligands and the solvent molecules were idealized with the standard SHELXL-93 idealization methods. The hydrogen atoms of water were directly located from a difference Fourier and included in least-squares as isotropic contributors. A modified[12] version of the absorption correction program DIFABS was applied. Brief crystal data for [Na(18C6)(H_2O)$_2$][Fe(TPP)(N_3)$_2$]·2C_6H_5Cl at both temperatures are listed in Table 1. Complete details of both structure determinations are available in the Supporting Information.

Table 1. Crystallographic Details for [Na(18C6)(H_2O)$_2$][Fe(TPP)(N_3)$_2$]·2C_6H_5Cl

	130 K	293 K
formula	$C_{68}H_{66}Cl_2FeN_{10}NaO_8$	
fw	1301.05	
a, Å	11.417(2)	11.7652(12)
b, Å	12.371(4)	12.6488(6)
c, Å	12.628(2)	12.8608(13)
α, deg	64.30(2)	62.02(2)
β, deg	77.18(3)	75.996(7)
γ, deg	77.67(2)	75.465(9)
V, Å^3	1553.0(6)	1618.8(2)
Z	1	
space group	$P\bar{1}$	
D_c, g/cm^3	1.391	1.335
μ, mm^{-1}	0.402	0.386
$\bar{\lambda}$, Å	0.710 73	
T, K	130(2)	293
final *R* indices[a] [$I > 2\sigma(I)$]	$R_1 = 0.0417$; $wR_2 = 0.1021$	$R_1 = 0.0688$; $wR_2 = 0.1750$
final *R* indices (for all data)	$R_1 = 0.0491$; $wR_2 = 0.1082$	$R_1 = 0.0933$; $wR_2 = 0.1983$

[a] $R_1 = \sum||F_o| - |F_c||/\sum|F_o|$ and $wR_2 = \{\sum[w(F_o^2 - F_c^2)^2]/\sum[wF_o^4]\}^{1/2}$. The conventional *R*-factors R_1 are based on *F*, with *F* set to zero for negative F^2. The criterion of $F^2 > 2\sigma(F^2)$ was used only for calculating R_1. *R*-factors based on F^2 (wR_2) are statistically about twice as large as those based on *F*, and *R*-factors based on *all* data will be even larger.

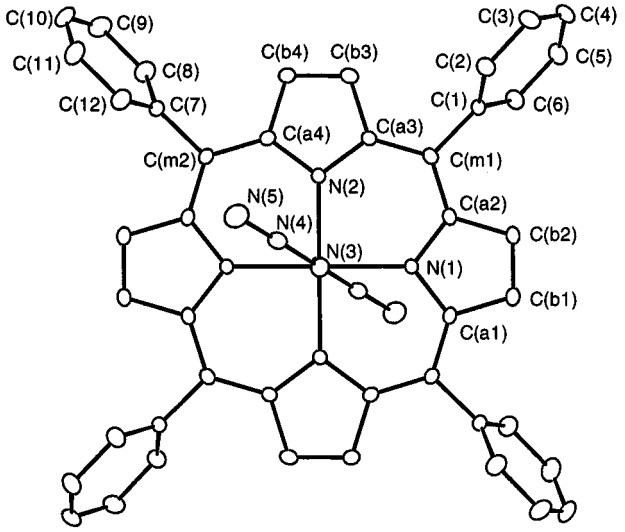

Figure 1. ORTEP diagram of [Fe(TPP)(N_3)$_2$]$^-$, view perpendicular to the porphyrin plane, showing the atom-labeling scheme for the unique half of the molecule. Thermal ellipsoids are drawn at the 50% probability level for the structure determined at 130 K.

Magnetic Susceptibility Measurements. Solid-state magnetic susceptibilities were measured under helium on a SHE Corp. VTS SQUID susceptometer from 5.5 to 301 K at a field of 0.5 T. The samples were contained in a Kel-F bucket, and they were purged by circulating helium gas in the antechamber for 0.5 h, rather than by the usual pump−purge cycles, in order to minimize the loss of chlorobenzene solvent molecules. The bucket had been calibrated independently at the same field and temperatures. Each raw data file was corrected for the diamagnetic contribution of both the sample holder and the compound to the susceptibility, using Pascal's constants for the metal axial ligands, counterion, and solvate molecules and a value of $\chi_M = -481 \times 10^{-6}$ cgs emu for H_2TPP.

Results

X-ray Structures. The structure of [Na(18C6)(H_2O)$_2$][Fe(TPP)(N_3)$_2$]·2C_6H_5Cl has been determined at 130(2) and 293 K. Figure 1 is an ORTEP diagram of the [Fe(TPP)(N_3)$_2$]$^-$ anion at 130 K. The labeling scheme is consistent in all of the ORTEP

(6) Adler, A. D.; Longo, F. R.; Finarelli, J. D.; Goldmacher, J.; Assour, J.; Korsakoff, L. *J. Org. Chem.* **1967**, *32*, 476.
(7) (a) Adler, A. D.; Longo, F. R.; Kampus, F.; Kim, J. *J. Inorg. Nucl. Chem.* **1970**, *32*, 2443. (b) Buchler, J. W. In *Porphyrins and Metalloporphyrins*; Smith, K. M., Ed.; Elsevier Scientific Publishing: Amsterdam, The Netherlands, 1975; Chapter 5.
(8) Gismelseed, A.; Bominaar, E. L.; Bill, E.; Trautwein, A. X.; Winkler, H.; Nasri, H.; Doppelt, P.; Mandon, D.; Fischer, J.; Weiss, R. *Inorg. Chem.* **1990**, *29*, 2741.
(9) Scheidt, W. R.; Turowska-Tyrk, I. *Inorg. Chem.* **1994**, *33*, 1314.
(10) Sheldrick, G. M. *Acta Crystallogr.* **1990**, *A46*, 467.
(11) Sheldrick, G. M. *J. Appl. Crystallogr.*, manuscript in preparation.
(12) The process is based on an adaptation of the DIFABS[13] logic to area detector geometry by Karaulov: Karaulov, A. I.; School of Chemistry and Applied Chemistry, University of Wales, College of Cardiff, Cardiff CF1 3TB, U.K., personal communication.
(13) Walker, N. P.; Stuart, D. *Acta Crystallogr., Sect. A* **1983**, *A39*, 158.

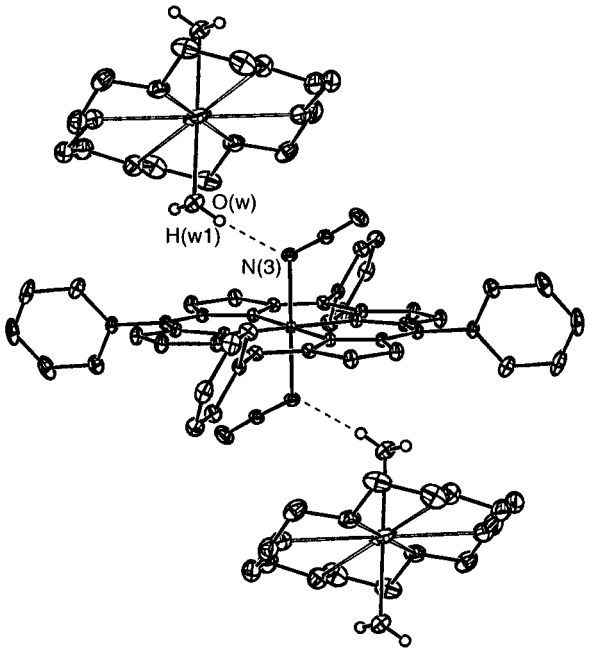

Figure 2. ORTEP diagram of $[Na(18C6)(H_2O)_2][Fe(TPP)(N_3)_2]$ showing the hydrogen-bonding network in the lattice. Thermal ellipsoids are drawn at the 50% probability level. The solvent molecules and hydrogen atoms have been omitted for clarity.

diagrams and tables. The iron of the $[Fe(TPP)(N_3)_2]^-$ anion and the sodium of the $[Na(18C6)(H_2O)_2]^+$ cation have crystallographically required inversion symmetry. Figure 2 shows the spatial arrangement of the $[Na(18C6)(H_2O)_2]^+$ cation as well as the anion. This figure clearly shows the linearity of the azide ligands. The dihedral angle of the 24-atom porphyrin core and the plane of the crown defined by the six oxygen atoms is 52°. The sodium cation is eight coordinate; six oxygen atoms of the crown ether and two oxygen atoms of water complete the coordination sphere. The distance between the water molecule oxygen and the coordinated azide nitrogen atom is 2.89 Å. The O(w)−H(w1)−N(3) angle is 170°. The average bond parameters for the unique half of the porphyrin core are depicted in Figure 3 along with the perpendicular displacements from the 24-atom mean plane. Selected bond lengths and angles are listed in Table 2. Complete listings of bond distances and angles for both structure determinations are included in the supporting information.

Physical Measurements. A powdered sample of $[Fe(TPP)(N_3)_2]^-$ at 77 K gives a rhombic EPR signal with g values of ∼1.82, 2.18, and 2.68. Figure 4 shows a 4.2 K spectrum with a fit generated by a three-term crystal-field model developed by one of us (CES) that includes the lowest quartet, $^4T_1$, and the single sextet, $^6A_1$, of the $3d^5$ configuration in addition to the low doublet $^2T_2$.[5] A predominantly cubic crystal field is assumed here, and other multiplets that are higher in energy have been ignored. The figure caption lists the spin−orbit coupling and Racah parameters used in these calculations as well as the crystal field and other parameters obtained in the fit. The principal g values were found to be 1.81, 2.18, and 2.70, and the energy splitting between the ground doublet and the (highly rhombic) sextet was ∼655 cm^{-1}, while the higher doublets of the $^2T_2$ manifold followed at ∼1000 and ∼2400 cm^{-1}, respectively. The quartets were at still higher energies but had a 0.9% admixture in the ground doublet as opposed to the 0.3% admixture of the sextet.

The single-crystal EPR measurements revealed an orientation of the **g**-tensor with no simple relation to the directions Fe−N(1), Fe−N(2), and Fe−N(3) of the iron site, in contrast to the

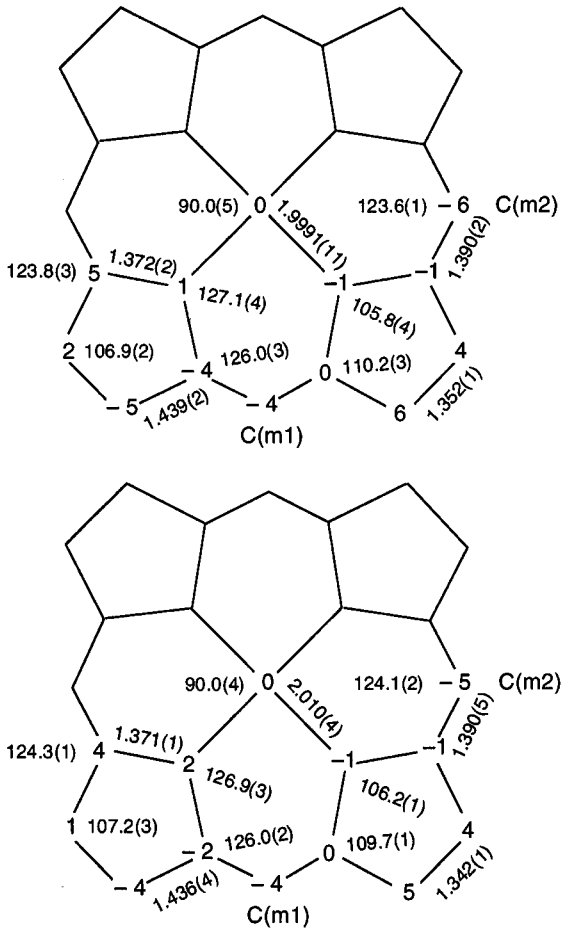

Figure 3. Formal diagrams of the porphyrinato core of $[Fe(TPP)(N_3)_2]^-$ at 130 K (top) and at 293 K (bottom). Shown are the perpendicular displacements, in units of 0.01 Å, from the 24-atom mean plane of the porphyrin core. In these centrosymmetric diagrams the symmetry-related atom has a displacement that is equal in magnitude but opposite in sign. Also shown are the average values for the bond parameters.

Table 2. Selected Bond Distances (Å) and Angles (deg) for $[Na(18C6)(H_2O)_2][Fe(TPP)(N_3)_2]\cdot 2C_6H_5Cl$[a,b]

lengths	130 K	293 K
Fe−N(1)	1.9999(12)	2.013(2)
Fe−N(2)	1.9983(13)	2.007(2)
Fe−N(3)	1.9734(14)	1.998(2)
N(3)−N(4)	1.206(2)	1.195(3)
N(4)−N(5)	1.150(2)	1.135(4)
angles	**130 K**	**293 K**
Fe−N(3)−N(4)	118.01(10)	118.9(2)
N(3)−N(4)−N(5)	177.2(2)	178.1(3)
N(3)−Fe−N(1)	89.45(5)	89.29(10)
N(3)−Fe−N(2)	90.60(6)	90.25(9)
N(3)−Fe−N(1)′	90.55(5)	90.70(10)
N(3)−Fe−N(2)′	89.40(6)	89.75(9)

[a] Estimated standard deviations of least significant digits are given in parentheses. [b] Primed atoms are generated by the symmetry transformation $-x, -y, -z$.

case of other low-spin iron porphyrins, which have g_{max} roughly along the normal to the porphyrin plane.[14] Specifically, the principal axes along g_{max} (g_{min}) have angles of ∼35° (77°) from Fe−N(1), ∼81° (38°) from Fe−N(2), and ∼56° (56°) from Fe−N(3). The projection of the azides onto the porphyrin plane also shows no simple relation to the axes of the **g**-tensor.

(14) Palmer, G. In *Iron Porphyrins*; Lever, A. B. P., Gray, H. B., Eds.; Addison-Wesley: Reading, MA, 1983; Vol. 2, Chapter 2.

Table 3. Selected Bond Distances (Å) and Angles (deg) for Iron(III) Porphyrinates[a]

compd	spin state	T (K)	Fe−N_p	Fe−N_{az}	Fe−N−N	ref
$Fe(TPP)N_3$	high	293	2.066(3)	1.953(5)	121.8(4)	23
$Fe(OEP)N_3$	high	130	2.056(2)	1.9618(14)	123.64(12)	*b*
$[Fe(TPP)(N_3)_2]^-$		293	2.010(4)	1.998(2)	118.9(2)	*c*
$[Fe(TPP)(N_3)_2]^-$		130	1.9991(11)	1.9734(14)	118.01(10)	*c*
$Fe(TPP)(Py)N_3$	low	293	1.989(6)	1.925(7)	125.6(7)	16
$Fe(TPP)(1\text{-}MeIm)N_3$	low	293	1.988(5)	1.931(5)	122.3(5)	23
$Fe(TPP)(1,2\text{-}Me_2Im)N_3$	low	293	1.983(8)	1.934(8)	121.6(7)	23
$[Fe(TPP)(CN)_2]^-$	low	293	2.000(6)	1.975(2)[d]		18
$[Fe(TPP)(F)_2]^-$	high	293	2.064(3)	1.966(2)[e]		22

[a] Estimated standard deviations of least significant digits are given in parentheses. [b] Unpublished results. [c] This work. [d] Fe−C. [e] Fe−F.

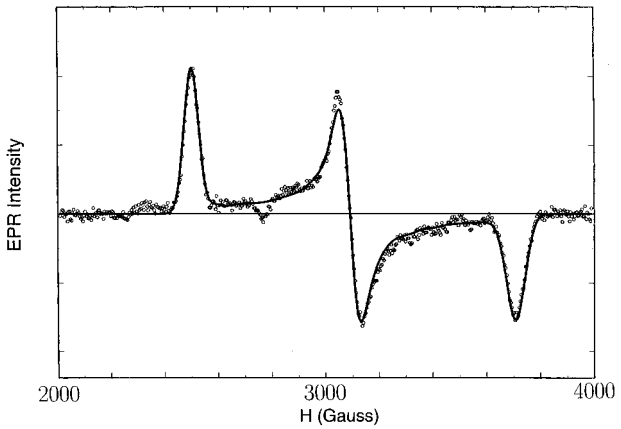

Figure 4. EPR powder spectrum of $[Na(18C6)(H_2O)_2][Fe(TPP)(N_3)_2]$ (circles) with superimposed simulation (solid line). Experimental conditions: 4.2 K, 0.2 μW at 9.44 GHz, 100 kHz modulation of 2 G amplitude, sweep rate 2 G/s, 5 sweeps. The simulation was based on the three-term model described in the text. The spin−orbit coupling and Racah parameters were taken as (all energies in cm^{-1}) $\lambda = 310$, $B = 1015$, and $C = 4800$, and the following values were used for the adjustable parameters: orbital reduction factor = 1.000, cubic splitting $10Dq = 35724$, $\sigma(10Dq) = 0.8$; second and fourth order axial fields $V_2 = 208$, $V_4 = -62$, $\sigma(V_4) = 1.65$; rhombic field $R = 159$, $\sigma(R) = 1.2$; intrinsic line width $\sigma_0 = 26$ G.

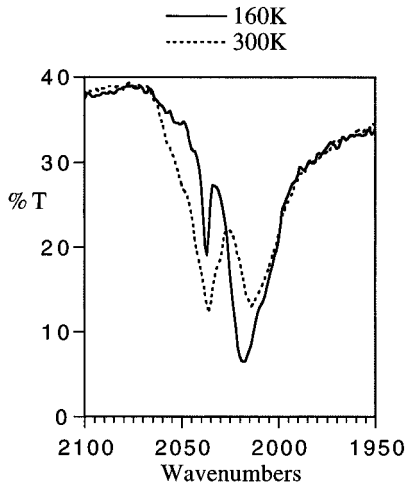

Figure 5. Infrared spectra of a KBr pellet of $[Fe(TPP)(N_3)_2]^-$ at 160 and 300 K. Shown are the azide asymmetric absorption bands.

The infrared spectra of the $[Fe(TPP)(N_3)_2]^-$ ion as a KBr pellet were recorded at ~300 and 160 K. The pellet was cooled by a N_2 gas stream flowing through coiled copper tubing immersed in liquid N_2. Figure 5 shows the azide asymmetric stretching region of these two spectra. The ratio of intensities of the two bands changes with temperature.

^{57}Fe Mössbauer absorption spectra were taken at several temperatures ranging from 4.2 to 300 K at zero applied field as well as in a 2.2 kG field. At higher temperatures two broad asymmetric lines were discernible but were better resolved in weak field. The two could be fitted, for $T > 120$ K, by a pair of Lorentzians of equal areas but unequal widths, Γ. Table 4 lists the quadrupole splittings, $\Delta E_q(T)$, and the effective line widths $\Gamma(T)$ obtained from the fits. The listed values of $\Gamma(T)$ exceed the minimum instrumental width of $\Gamma_0 = 0.25$ mm/s as a result of residual magnetic hyperfine interaction. As Figure 6 illustrates, ΔE_q is constant at 2.33 mm/s up to roughly 150 K, but above 150 K ΔE_q decreases gradually to 1.71 mm/s at 300 K.

Table 4. Quadrupole Splitting, ΔE_q, and Effective Line Width, Γ, as a Function of Temperature[a]

T (K)	ΔE_q[b,c]	Γ_1[b,c]	Γ_2[b,c]
140	2.296(50)	0.77(1)	0.67(1)
150	2.294(50)	0.69(1)	0.62(1)
160	2.317(30)	0.647(12)	0.591(12)
175	2.250(10)	0.540(8)	0.527(8)
180	2.288(10)	0.519(6)	0.518(7)
200	2.224(20)	0.444(6)	0.458(8)
225	2.127(40)	0.379(6)	0.401(8)
250	2.062(20)	0.354(6)	0.387(8)
275	1.918(5)	0.321(6)	0.335(8)
294	1.823(10)	0.316(6)	0.356(8)
302	1.711(30)	0.368(10)[d]	

[a] In a perpendicular field of 2.2 kG. [b] In mm/s. [c] Uncertainty in units of the least significant figure. [d] Constrained to be equal.

At 4.2 K, magnetic hyperfine splittings are resolved in fields of several kilogauss, but still higher fields are needed to minimize the effects of spin fluctuation. Figure 7 shows a Mössbauer spectrum recorded at 8.5 T and 4.2 K and a superimposed spectral simulation with the parameters listed in the caption. The simulation is based on the spin Hamiltonian:[15]

$$H = \mu_B \mathbf{S}\cdot\mathbf{g}\cdot\mathbf{B} + \mathbf{S}\cdot\mathbf{A}\cdot\mathbf{I} + \mathbf{I}\cdot\mathbf{P}\cdot\mathbf{I} - \mu_N g_N \mathbf{I}\cdot\mathbf{B} \quad (1a)$$

$$\mathbf{I}\cdot\mathbf{P}\cdot\mathbf{I} = (eQ/6)(V_{\xi\xi}I_\xi^2 + V_{\eta\eta}I_\eta^2 + V_{\zeta\zeta}I_\zeta^2) \quad (1b)$$

Here **g** is the **g**-tensor measured by EPR, **A** is the magnetic hyperfine tensor, and **P** is the quadrupole tensor. The principal axes of **g** and **A** are assumed to be the same, but **P** is allowed to have different axes which are obtained from those of **g** or **A** by a rotation with Euler angles α, β, γ. The simulation of Figure 7 reproduces the data reasonably well, but the reliability of the resulting spin Hamiltonian parameters is limited by the counting statistics of the data. It does not depend on the spin fluctuation rate, however, as the limits of fast or slow fluctuations produce indistinguishable spectra under the experimental conditions. We note that a finite Euler angle $\alpha = -39°$ improves the simulation noticeably, whereas a second angle β does not, hence β and γ are kept equal to zero. The asymmetry parameter η is defined as $\eta = (V_{\xi\xi} - V_{\eta\eta})/V_{\zeta\zeta}$, and the value found, $\eta = 1.8$, implies

(15) Debrunner, P. G. In *Iron Porphyrins*; Lever, A. B. P., Gray, H. B., Eds.; VCH Publishers: New York, 1989; Vol. 3, p 137.

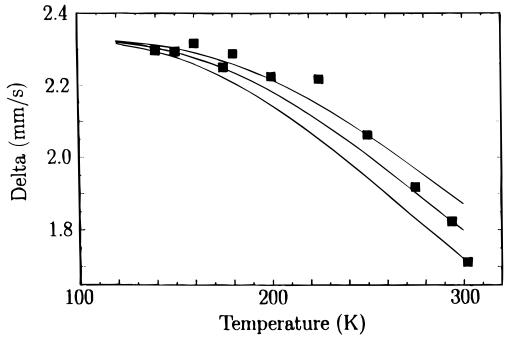

Figure 6. Quadrupole splitting, ΔE_q, versus temperature. The solid lines are model predictions adjusted to match $\Delta E_q(302)$, $\Delta E_q(294)$ and $\Delta E_q(250)$, respectively, as described in the text.

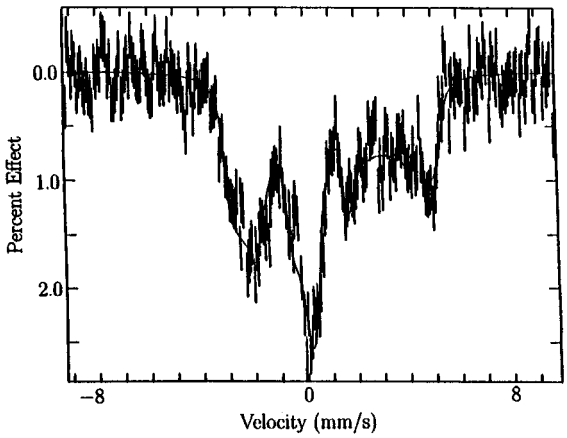

Figure 7. Mössbauer spectrum of $[Na(18C6)(H_2O)_2][Fe(TPP)(N_3)_2]$ at 4.2 K in a field of 8.5 T parallel to the γ beam. The solid line is a fit based on a spin $S = {}^1/_2$ Hamiltonian discussed under Results with $\mathbf{g} = (1.81, 2.18, 2.70)$, $\mathbf{A}/\mu_N g_N = (-24, -1.31)$T, $\Delta E_q = 2.33$ mm/s, $\eta = 1.8$, and $\alpha = -39°$ (=first Euler angle rotating from the **g** or **A** frame to the frame of the quadrupole tensor, $\beta = \gamma = 0$).

that $V_{\eta\eta} = -V_{\zeta\zeta}(\eta + 1)/2$ is the component of largest magnitude and is negative. A 90° rotation about ξ changes this "improper coordinate system" into a proper one with a smaller asymmetry parameter of 0.429.

Magnetic susceptibilities were measured for the bis(azide) complex from 5.5 to 301 K. A plot of μ_{eff} vs temperature is given in Figure 8. Initial measurements showed that the samples readily lost chlorobenzene. Accordingly, subsequent samples were purged by circulating helium gas in the antechamber for 0.5 h, rather than by the usual pump−purge cycles, in order to minimize loss of chlorobenzene solvate molecules. The effective magnetic moments were calculated from the equation $\mu_{eff} = 2.84(\chi_M T)^{1/2}$, where χ_M is the corrected molar susceptibility and T is the temperature.

Discussion

Synthesis. The bis(azido)(porphinato)iron(III) anion, $[Fe(Porph)(N_3)_2]^-$, has been prepared with the porphyrin ligands, TPP, $T_{piv}PP$, and TMP. We have used the synthetic strategy of crown-ether-solubilized sodium azide to increase the concentration of azide ion in these organic solvent preparations. Crystallization of the anionic product may be aided by the relatively large cationic sodium crown ether. The preparation of these six-coordinate complexes is easily confirmed by the presence of a low-spin rhombic EPR signal for the frozen solutions at 77 K. Only the five-coordinate azide has been isolated when OEP was used as the porphyrin ligand. The increased basicity of this porphyrin may significantly decrease the binding constant for the second azide ion. For all the other

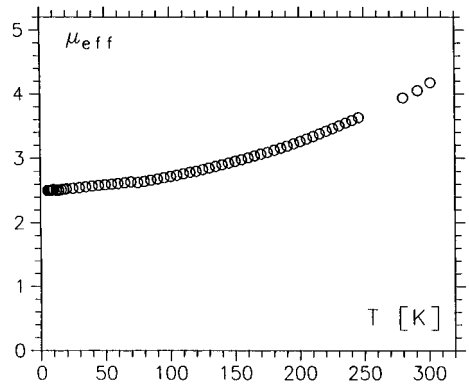

Figure 8. Temperature dependence of the magnetic moment of $[Fe(TPP)(N_3)_2]^-$.

porphyrins, the six-coordinate anionic species is unstable with respect to the five-coordinate neutral species in dilute solutions even when the concentration of free azide is high. It should be noted that the five-coordinate azido species can easily be made without the use of the crown ether strategy.[16,17]

The initial powder EPR parameters and the appearance of two asymmetric azide stretches in the IR suggested that the complex might have particularly interesting electronic properties. Accordingly, we have characterized the $[Fe(TPP)(N_3)_2]^-$ species with a variety of methods over a range of temperatures. As described below, all physical measurements are consistent with the presence of a spin equilibrium. Indeed, all of the six-coordinate azide derivatives listed above display EPR and IR data consistent with a spin-equilibrium system. Crystalline $[Fe(T_{piv}PP)(N_3)_2]^-$ derivatives were profoundly disordered and single crystals of the $[Fe(TMP)(N_3)_2]^-$ anion could not be obtained. Accordingly, neither system was investigated in further detail.

Finally, we note that the application of similar synthetic strategies with the pseudohalides cyanate and thiocyanate did not yield species with any low-spin EPR signal in frozen solution at either 77 or < 20 K. These systems have not been investigated further.

Structures. Structure determinations for $[Na(18C6)(H_2O)_2][Fe(TPP)(N_3)_2]\cdot 2C_6H_5Cl$ were performed at 293 K and at 130 K using the same crystal specimen. The same data collection methods were used with requisite modifications due to the temperature difference. An overall view of the structure at 130 K is given in Figure 2. The iron atom is required by symmetry to lie in the plane of the porphyrin, and as shown in Figure 3, the core is essentially planar. The structural parameters are entirely consistent with those expected for a low-spin, anionic iron(III) porphyrinate.[18] The average $Fe-N_p$ bond length in the centrosymmetric complex is $Fe-N_p = 1.9991(11)$ Å, essentially the same as that in the anionic dicyano derivative[18] and slightly longer than those of the neutral, low-spin species listed in Table 3. The small differences in $Fe-N_p$ are the expected effects of charge on the complex and core conformation.

The coordinated azide ion is linear; the two N−N distances are inequivalent. The longer bond occurs between the central nitrogen and the coordinated nitrogen atom. This difference is not unusual and reflects one resonance form of bound azide.

(16) Adams, K. M.; Rasmussen, P. G.; Scheidt, W. R.; Hatano, K. *Inorg. Chem.* **1979**, *18*, 1892.
(17) Byers, W.; Cossham, J. A.; Edwards, J. O.; Gordon A. T.; Jones, J. G.; Kenny, E. T. P.; Mahmood, A.; McKnight, J.; Sweigart, D. A.; Tondreau, G. A.; Wright, T. *Inorg. Chem.* **1986**, *25*, 4767.
(18) Scheidt, W. R.; Haller, K. J.; Hatano, K. *J. Am. Chem. Soc.* **1980**, *102*, 3017.

The Fe−azide plane makes a dihedral angle of 32° with the plane defined by Fe, N(1), and N(3) (see Figure 1). The axial Fe−N_{az} bond length is 1.9734(14) Å. This distance is quite long compared to the neutral, mixed-ligand, low-spin azido complexes in Table 3 and likely reflects the decreased attraction of iron(III) for a second anionic, axial ligand. It is also slightly longer than the five-coordinate Fe−N_{az} bond length. The 118.01(10)° Fe−N(3)−N(4) angle is significantly smaller than that in either the five-coordinate, high-spin or six-coordinate, low-spin complexes but is within the range for the angle of a trigonally hybridized nitrogen. Crystal packing effects may significantly influence the value of this angle.

The charge of the $[Fe(TPP)(N_3)_2]^-$ anion is balanced by a sodium cation coordinated by 18C6 and two water molecules. The water oxygen atoms of the cation are within hydrogen bonding distance[19] to the coordinated azide nitrogens with O(w)···N(3) distances of 2.89 Å as seen in Figure 2. The O(w)−H(w1)−N(3) angle of 170° is also consistent with a significant hydrogen bond. This hydrogen bonding pattern forms a continuous chain-like arrangement of atoms (−Fe−N−H−O−Na−O−H−N−Fe−) in the cell. Figure 2 shows this quite well. We believe that this hydrogen bonding interaction modulates the crystal field strength of the azide ligands modestly and is a contributing factor to the observed spin-equilibrium phenomena.

If the $[Fe(TPP)(N_3)_2]^-$ complex anion is a high-spin−low-spin spin-equilibrium system, its structure should be temperature dependent; increasing the temperature ought to increase the bond distances around iron. The 293 K structure determination shows that there are increases in both the Fe−N_p bond lengths and the Fe−N_{az} bond lengths compared to the 130 K structure. The values are tabulated in Table 3. Although the Fe−N_p difference is not large enough to be statistically significant, the effect is in the appropriate direction. Moreover, the magnitude of the changes are consistent with that expected from the other physical measurements.

It is well-known that the equatorial Fe−N_p bond lengths are dependent on the spin state.[20] The differences in the equatorial bond lengths (radial expansion of the porphyrin core) can be used to calculate approximately the fraction of the two spin states present.[21] A reasonable upper limit for the high-spin Fe−N_p bond length is that of a pure high-spin, planar, six-coordinate, anionic species such as $[Fe(TPP)(F)_2]^-$ (2.064(3) Å).[22] The low-spin limit used is that of the pure low-spin, six-coordinate species $[Fe(TPP)(CN)_2]^-$ (2.000(6) Å).[18] A calculation of spin-state fraction based on those limits yields an estimate of 17% high-spin state at room temperature. The axial Fe−N_{az} bond distance increase of 0.025 Å is also consistent with some fraction of high-spin species present. The linear extrapolation of distances can be used to estimate the axial Fe−N_{az} bond distance for a pure high-spin complex (2.120 Å).

Infrared Spectroscopy. Transition metal azide complexes exhibit an intense infrared absorption band around 2000 cm^{-1} corresponding to the asymmetric azide stretch. Two asymmetric azide stretches (2036 and 2014 cm^{-1}) are present in the infrared spectrum of crystalline $[Fe(TPP)(N_3)_2]^-$. These absorption bands can be assigned to the high- and low-spin species, respectively. The temperature dependence of these two bands was investigated, and Figure 5 shows their temperature dependence. As would be expected, the intensity of the 2014 cm^{-1} band increases and the 2036 cm^{-1} band correspondingly decreases upon cooling.

McCoy and Caughey[24] observed infrared bands for MbN_3 at 2045 and 2023 cm^{-1} and at 2047 and 2025 cm^{-1} for HbN_3 in aqueous solution; both of these hemoprotein systems are spin-equilibrium systems with azide and histidine as the ligand set. On the basis of the frequencies and the ratio of intensities of these bands, the band at 2045 cm^{-1} was assigned to the high-spin form and the 2023 cm^{-1} band to the low-spin form. Alben and Fager subsequently confirmed this assignment.[25] In addition, they also showed that the ratio of intensities of these two bands is temperature dependent. The band at 2046 cm^{-1} increases and the band at 2023 cm^{-1} decreases as the temperature is raised. The IR observations for $[Fe(TPP)(N_3)_2]^-$ are in clear agreement with these earlier hemoprotein assignments.

Mössbauer Spectroscopy. We have used variable-temperature ^{57}Fe Mössbauer spectroscopy to further study the spin-equilibrium process. The low-field Mössbauer parameters obtained for the bis(azide) species at various temperatures are given in Table 4. Figure 6 illustrates the monotonic decrease of the quadrupole splitting, ΔE_q, from its low-temperature value of 2.33 to 1.71 mm/s at 300 K (73% of the maximum). A decrease of this magnitude is quite unusual for low-spin ferric porphyrins and strongly suggests a dynamic process, in the simplest case a thermal admixture of the high-spin $S = {}^5/_2$ state with rapid interconversion between the two multiplets. With few exceptions, high-spin ferric porphyrins have smaller, positive quadrupole splittings in the range of (1 ± 0.5) mm/s, and a rapid interconversion of the low- and high-spin states will therefore result in an averaged ΔE_q that decreases with increasing temperature. As can be seen in Table 4, the relatively small line width at the higher temperatures is compatible with rapid interconversion.

In order to assess the feasibility of a model based on thermal excitation of the $S = {}^5/_2$ state we will assume that all M_S sublevels, say at the energy Δ above the $S = {}^1/_2$ state, are equally populated, and we simply substitute thermal expectation values, $\langle -V_{ii}\rangle_T$, $i = 1, 2, 3$, of the principal components of the EFG tensor into the expression for the quadrupole splitting, $\Delta E_q = [eQ/\sqrt{6}][\sum(\langle -V_{ii}\rangle_T)^2]^{1/2}$, with $\langle -V_{ii}\rangle_T = [V_{ii}({}^1/_2) + 3V_{ii}({}^5/_2)\exp(-\Delta/T)]/[1 + 3\exp(-\Delta/T)]$. The EFG tensor of the ground doublet, $V_{ii}({}^1/_2)$, is known from the high-field measurements at 4.2 K (see below), but $V_{ii}({}^5/_2)$ can only be guessed. Assuming the simple case of $V_{ii}({}^5/_2) = -V_{ii}({}^1/_2)/2$, $\eta = 0$, hence $\Delta E_q({}^5/_2) = +1.16$ mm/s, we obtain the solid lines in Figure 6, where the values of Δ/k were taken to be 796, 845, and 897 K in order to match the data points at 302, 294, and 250 K, respectively. As can be seen from Figure 6, the general trend of $\Delta E_q(T)$ is well produced by the model, but none of the three curves matches the experimental slope at high temperatures. It appears, therefore, that the dynamics of the process is more complex than our simple model assumes, and vibronic effects may be involved as discussed for a related case by Bominaar and Block.[26] The energy difference between doublet and sextet, $\Delta \approx 590$ cm^{-1}, is quite close to the used independently in the EPR simulation in Figure 4[27] and is also comparable to the estimate of 17% high spin at 293 K from the X-ray data.[28]

The high-field, low-temperature spectrum of Figure 7 allows a detailed analysis of the hyperfine interactions of the ^{57}Fe

(19) Ibers, J. A.; Hamilton, W. A. *Hydrogen Bonding in Solids*: New York, 1968.
(20) Scheidt, W. R.; Reed, C. A. *Chem. Rev.* **1981**, *81*, 543.
(21) Scheidt, W. R.; Geiger, D. K.; Haller, K. J. *J. Am. Chem. Soc.* **1982**, *104*, 495.
(22) Scheidt, W. R.; Lee, Y. J.; Tamai, S.; Hatano, K. *J. Am. Chem. Soc.* **1983**, *105*, 778.
(23) Zhang, Y.; Hallows, W. A.; Ryan, W. J.; Jones, J. G.; Carpenter, G. B.; Sweigart, D. A. *Inorg. Chem.* **1994**, *33*, 3306.
(24) McCoy, S.; Caughey, W. S. *Biochemistry* **1970**, *9*, 2387.
(25) Alben, J. O.; Fager, L. Y. *Biochemistry* **1972**, *11*, 842.
(26) Bominaar, E. L.; Block, R. *J. Chem. Phys.* **1991**, *95*, 6712.

nucleus with the surrounding electron distribution, specifically the 3d-electrons. As indicated by the solid line in Figure 7, the spectrum has been simulated successfully in terms of the spin Hamiltonian (1), and we will now consider the interpretation of the hyperfine tensors **A** and **P** on the basis of Lang's extension of the Griffith model.[29] Given the *g*-values from EPR, this model calculates the wave function of the unpaired electron and, using some semiempirical parameters, predicts the following **A**-tensor, $\mathbf{A}/\mu_N g_N = P$ (−0.73, 0.10, 0.57)T, where $\kappa = 0.35$ has been assumed and the scale factor *P*, proportional to $\langle r^{-3} \rangle$ of the unpaired electron, normally has the value of 64 T. To optimize the agreement with the fitted values, however, the overall factor *P* has to be reduced by a factor of roughly $^5/_8$ to $P \approx 40$ T, giving an **A**-tensor $\mathbf{A}/\mu_N g_N = (-29.3, 3.8, 22.9)$T. A_1 and A_3 are close to the empirical values given in the caption of Figure 7, while A_2, which is smaller and therefore quite uncertain, is off by 5 T. The important point here is that the reduction of *P* indicates very strong delocalization of the unpaired electron in keeping with the covalency of the iron−nitrogen bonds. The same crystal field model predicts a quadrupole tensor $(eQ/2)(V_{\xi\xi},V_{\eta\eta},V_{\zeta\xi}) = R(-0.95, 0.46, 0.50)$, where the scale factor *R* typically has the value of ∼3 mm/s. Both the negative sign and the approximate size of the largest tensor component $V_{\xi\xi} = -2.86$ mm/s, match the empirical values discussed under Results, but the fits showed the component of largest magnitude to be $V_{\eta\eta} = -2.26$ mm/s albeit with a rotation by $\alpha = -39°$ from the principal axes implied here. Since the model ignores covalency effects, which should be particularly important in $[Fe(TPP)(N_3)_2]^-$, no better agreement can be expected.

EPR and Magnetic Properties. $[Fe(TPP)(N_3)_2]^-$ gives an EPR spectrum that is generally typical of rhombic, low-spin iron(III) porphyrinates. Calculation of the tetragonality and rhombicity parameters from the *g* values by Taylor's method[30] gives values of $\Delta/\lambda = 6.26$ and $V/\Delta = 0.45$, respectively. In the Blumberg/Peisach coordinate system,[31] the tetragonality and rhombicity parameters are −5.24 and −0.92.[32] Interestingly, the tetragonality and rhombicity parameter values do not fall within the bis(nitrogen ligand) class (i.e., H-type, azide- or histidine-substituted myoglobins or hemoglobins), as might have been expected, but rather close to class O (i.e., hydroxy-substituted hemoproteins). The picket-fence derivative gives similar crystal field values ($\Delta/\lambda = -5.71$ and $V/\Delta = -0.98$) in the Blumberg/Peisach coordinate system. The novelty of these EPR-derived crystal field parameters then led us to more detailed studies.

Taylor's reformulation of the Griffith model[33] considers the $^2T_2$ manifold of the $(3d)^5$ configuration only and is therefore unable to describe the low-spin/high-spin equilibrium suggested by the structural, magnetic, and Mössbauer data of $[Fe(TPP)(N_3)_2]^-$. Nevertheless, admixtures of higher spin multiplets are known to affect the low-spin *g*-values, in particular those of class P compounds,[34,35] which otherwise require orbital reduction factors in excess of 1 and/or imply unnormalizable wave functions.[5] We have therefore used an extension of the $^2T_2$ crystal field model that also includes the next higher terms $^4T_1$ and $^6A_1$ as suggested by Ristau. Figure 4 illustrates that a good fit of the 4 K EPR powder spectrum can be obtained with this $(3d)^5$ model. The model has a large number of parameters, as listed in the caption of Figure 4. With the three *g*-values to be fit, the system is underdetermined and we have chosen to fix *B*, *C*, and λ. A final factor complicating the fit is the fact that the Mössbauer shows that the EFG and **g**-tensors are not coincident, and therefore, the crystal field symmetry is actually lower than rhombic. In spite of the large number of variables, however, it is by no means trivial to match the data as well as in Figure 4. The resulting parameters therefore deserve further discussion.

Of special interest is the prediction that the sextet is the first excited multiplet at ∼655 cm^{-1} although its admixture to the low doublet is only 0.3% and therefore lower than the 0.9% admixture to the much higher quartet. To compare the predictions of the three-term model with those of the simpler Griffith/Taylor model (which uses the orbital reduction factor as a variable and normalized wave functions), we note that the latter places the two higher doublets of the $^2T_2$ manifold at 967 and 2543 cm^{-1}, respectively, as opposed to 1009 and 2417 cm^{-1}, respectively, in the three-term model. Here, the same value of the spin−orbit coupling, $\lambda = 310$ cm^{-1}, has been adopted in both models. It is important to note that, in order to fit the *g*-values, the orbital reduction factor in the Griffith model was required to take the physically unmeaningful value of 1.07 while the three-term model used a value of 1.00.

Furthermore, single-crystal EPR experiments were done to define the orientation of the principal axes of the **g**-tensor relative to the porphyrin. In low-spin ferric porphyrins, the *g* -value of greatest magnitude is typically found within several degrees of the porphyrin normal, while the other two principal axes are near the porphyrin plane but may be rotated away from the $Fe-N_p$ vectors depending on the type and orientation of the axial iron ligands.[14,15,33,36,37] In $[Fe(TPP)(N_3)_2]^-$, on the other hand, the **g**-tensor is not only rotated about the porphyrin normal but in addition rotated away from it, as specified under Results. In fact, the angles from the porphyrin normal to the principal axes of the **g**-tensor are almost the same, that is 56° to g_1, 52° to g_2, and 56° to g_3. Barring any errors in the interpretation of the single crystal measurements, this unexpected result calls for a reexamination of the Griffith model, which describes the wave function of the unpaired electrons as a t_{2g} hole state in a crystal field of coaxial cubic, axial and rhombic components with spin−orbit coupling.[33] In this model the principal axes of the **g**-tensor coincide with the crystal field axes, in the simplest case of a D_{4h} porphyrin given by the $Fe-N_p$ vectors and the porphyrin normal. As Lang later showed, in lower symmetry the rhombic components of the crystal field may be rotated away from the $Fe-N_p$ vectors, and the **g**-tensor then rotates in a related fashion about the porphyrin normal.[36,37,38] Extending these ideas to the lower symmetry of $[Fe(TPP)(N_3)_2]^-$, none of the rhombic field axes are likely to be along the porphyrin normal, and the **g**-tensor may therefore assume a more general orientation as observed. The short Fe−N(3) distance indicates that the two azides have stronger σ- and

(27) Note that Δ deduced from the EPR simulation scales with the input energies *B*, *C*, and λ.
(28) The fractional population of the sextet is $0.17 = 1/[\exp(\Delta/293)/3 + 1]$ for $\Delta/k = 786$ K.
(29) Lang, G. *Quart. Rev. Biophys.* **1970**, *3*, 1.
(30) Taylor, C. P. S. *Biochim. Biophys. Acta* **1977**, *491*, 137.
(31) Blumberg, W. E.; Peisach, J. In *Probes of Structure and Function of Macromolecules and Membranes*; Chance B., Yonetani, T., Mildvan, A. S., Eds.; Academic Press: New York, 1971; Vol. 2, pp 215−229.
(32) See Palmer[14] for a discussion of the differences in the coordinate systems. The Blumberg−Peisach Truth diagrams are typically plotted using tetragonalities and rhombicities calculated using their coordinate definition.
(33) Griffith, J. S. *Nature (London)* **1957**, *180*, 30.
(34) Ruf, H. H.; Ahr, H.; Nastainczyk, W.; Ullrich, V.; Mansuy, D.; Battioni, J.-P.; Montiel-Montoya, R.; Trautwein, A. *Biochemistry* **1984**, *23*, 5300.
(35) Debrunner, P. G.; Dexter, A. F.; Schulz, C. E.; Xia, Y.-M.; Hager, L. P. *Proc. Natl. Acad. Sci. U.S.A.* **1996**, *93*, 12791.
(36) Soltis, S. M.; Strouse, C. E. *J. Am. Chem. Soc.* **1987**, *110*, 2824.
(37) Rhynard, D.; Lang, G.; Spartalian, K. J. *J. Chem. Phys.* **1979**, *71*, 3715.
(38) Oosterhuis, W. T.; Lang, G. *Phys. Rev.* **1969**, *178*, 439.

π-bonding to the iron than do the pyrrole nitrogens, and if these covalent bonds can be modeled by an effective rhombic crystal field component, that field may well be tilted away from the porphyrin normal and thus cause the **g**-tensor to rotate. In any case, it would be interesting to see if a more realistic molecular orbital calculation is able to rationalize the observations.

The preparation of a pure sample of $[Na(18C6)(H_2O)_2][Fe(TPP)(N_3)_2]\cdot 2C_6H_5Cl$ for magnetic susceptibility measurements presented a number of unexpected difficulties. Crystals of $[Na(18C6)(H_2O)_2][Fe(TPP)(N_3)_2]\cdot 2C_6H_5Cl$, obtained directly from the reaction mixture, are contaminated with a crown ether/sodium azide coating that could not be removed mechanically. Unfortunately, samples washed with water to remove the excess crown/sodium azide then contain a small amount of a high-spin impurity detectable by Mössbauer spectroscopy. Unwashed samples do not, however, show this Mössbauer-detectable impurity. A second problem was that the chlorobenzene solvate molecules (in spite of its relatively high boiling point) were easily lost from the crystalline lattice. Some solvent loss appeared in the susceptibility samples even when the SQUID chamber was purged rather than evacuated prior to the magnetic measurements. Thus, there is some experimental uncertainty in the formula weight of the sample. An attempt to eliminate all solvent in this system did not seem advisable as lattice solvation loss could lead to changes in magnetic properties. Such solvation effects have been seen previously for other iron(III) spin-equilibrium systems.[39−42] Finally grinding the sample may also raise the effective magnetic moment as has been previously seen.[43]

The measured magnetic moment for the bis(azide) complex from 5.5 K ($\mu_{eff} = 2.5\ \mu_B$) to 301 K ($\mu_{eff} = 4.2\ \mu_B$) is given in Figure 8. Replicate measurements on independently prepared samples gave qualitatively similar results. The complex is known from the Mössbauer studies to be low spin at low temperature; the expected value of the magnetic moment at 4.2 K can be calculated from the EPR g values to be 1.96 μ_B. Temperature-dependent magnetic measurements for low-spin iron(III) porphyrinate systems are very rare but appear to increase at higher temperature.[16] The somewhat larger than expected values of μ_{eff} observed at the lowest temperatures undoubtedly reflects the experimental difficulties described above. As can be seen from Figure 8, μ_{eff} increases significantly with temperature and provides a qualitative description and confirmation of the spin-equilibrium system. Application of the relationship $\mu_{obs}^2 = (1 - A)\mu_H^2 + A\mu_L^2$ provides an estimate of a 30−35% population of the high-spin state at room temperature. The relatively large uncertainty in these values is a reflection of the difficulties caused by uncertainty in the composition that results from the loss of solvent. This high-spin fraction estimate is larger than expected from the bond length measurements and represents an upper limit of the high-spin population.

Summary. The synthesis and characterization of an anionic iron(III) bis(azido) porphyrin derivative, $[Na(18C6)(H_2O)_2][Fe(TPP)(N_3)_2]\cdot 2C_6H_5Cl$, is described. The crown ether 18C6 was used to solubilize sodium azide and perhaps to stabilize the six-coordinate anionic porphyrin species. Temperature-dependent IR and Mössbauer spectra, and magnetic susceptibility data are all consistent with the complex being an $S = {}^1/_2 \rightleftharpoons S = {}^5/_2$ spin-equilibrium system. Structure determinations at 130 and 293 K show an expansion of the coordination group for the axial as well as equatorial bonds. An increasing proportion of a high-spin state is populated at higher temperature. A fit of the powder EPR spectrum suggests that the sextet is ∼655 cm^{-1} above the ground doublet. The spin-crossover rate is between the Mössbauer time scale (10^{-7} s) and the vibrational time scale (10^{-13} s). Single-crystal EPR spectra show that the **g**-tensor has an unusual orientation with respect to the coordinate system defined by the heme.

Acknowledgment. We thank the National Institutes of Health for support of this research under Grants GM-38401 (W.R.S.), GM-48513 (C.E.S.), and GM-16406 (P.G.D.). Funding for the purchase of the FAST area detector diffractometer was provided through NIH Grant RR-06709.

Supporting Information Available: Two X-ray crystallographic files, in CIF format, are available. Access information is given on any current masthead page.

IC970527L

(39) Sinn, E. *Inorg. Chem.* **1976**, *15*, 369.
(40) Butcher, R. J.; Sinn, E. *J. Am. Chem. Soc.* **1976**, *98*, 2440. Butcher, R. J.; Sinn, E. *J. Am. Chem. Soc.* **1976**, *98*, 5159.
(41) Cukauskas, E. J.; Deaver, B. S.; Sinn, E. *J. Chem. Phys.* **1977**, *67*, 1247.
(42) Malliaris, A.; Papaefthimiou, V. *Inorg. Chem.* **1982**, *21*, 770.
(43) Haddad, M. S.; Federer, W. D.; Lynch, M. W.; Hendrickson, D. N. *Inorg. Chem.* **1981**, *20*, 131.